Simultaneous composition and thickness measurement of paper using terahertz time-domain spectroscopy

Payam Mousavi,[1,*] Frank Haran,[2] David Jez,[2] Fadil Santosa,[3] and John Steven Dodge[1]

[1] *Department of Physics, Simon Fraser University,*
8888 University Dr., Burnaby, British Columbia, V5A 1S6, CANADA

[2] *Honeywell Process Solutions,*
500 Brooksbank Ave., North Vancouver, British Columbia, V7J 3S4, CANADA

[3] *Institute for Mathematics and its Applications (IMA), University of Minnesota,*
114 Lind Hall 207 Church Street S.E. Minneapolis, MN 55455-0134, USA

[*] *Corresponding author: pma23@sfu.ca*

We present a non-contact method for quantitative composition and thickness monitoring of flat sheet products using terahertz time-domain spectroscopy (THz-TDS). We apply the method to obtain simultaneous measurement of thickness and moisture content of paper sheets. The paper is modeled as an effective medium of water mixed with fibers, and model parameters are estimated from fits to the measured transmission amplitude. We demonstrate the method on two different paper samples and obtain uncertainties that are comparable with existing sensor technology. Monte Carlo simulations indicate that these uncertainties can be reduced further by at least an order of magnitude.

OCIS codes: 120.0120, 300.6495, 040.2235

1. Introduction

Terahertz spectroscopy [1, 2] has emerged as a potentially important tool for material characterization [3]. Early studies identified terahertz-frequency vibrational modes that could be used for chemical recognition and crude monitoring of hydration levels [4, 5]. More recent work has focused on exploiting terahertz absorption features for quantitative monitoring of material composition and hydration levels [6–10]. The majority of these studies rely on direct absorption measurements to determine the relative concentration of compounds with distinct vibrational frequencies, with the sample in vapor phase or diluted in a pellet of material that is transparent to terahertz radiation. For dense aqueous and amorphous mixtures, however, local field effects play a role and the vibrational spectra are extremely broad [10], so precise characterization with direct absorption is challenging.

Paper in its simplest form is a dense mixture of water and cellulose fiber, and presents a basic compositional analysis problem that can not be solved by monitoring vibrational lines in a diluted sample. Currently paper manufacturers use two separate gauges to measure thickness and moisture content [11]. A quantitative relationship between terahertz absorption and the water content of paper has been established, but this method does not provide an estimate of either the thickness or the weakly absorbing dry content [12]. Previous work has shown that terahertz spectroscopy is capable of measuring thickness and dielectric properties simultaneously [13, 14], but this has not yet been extended to compositional analysis. In this work, we offer a THz-TDS methodology to determine thickness and paper composition simultaneously, with accuracy comparable to existing sensor technology. Our method relies on fits of a physical model to the complex transmission amplitude of the sample over the full terahertz bandwidth, and is readily extended to similar problems in material characterization. Monte Carlo simulations based on a simple noise model show good agreement with experimental results, and indicate that the current uncertainties can be reduced further by an order of magnitude.

2. Model

We begin by presenting a physical model to relate the terahertz transmission amplitude of a paper sample to its thickness h and dry content volume fraction ν_d. For a given paper type, the moisture content M is determined from ν_d through a separate calibration of the density and refractive index of the dry content.

We model paper as a dielectric slab consisting of a heterogenous mixture of dry content and water, using the Bruggeman model to account for local field effects [15]. Given constituent permittivities $\varepsilon_d, \varepsilon_w$, and volume fractions ν_d, ν_w, for dry content and water, respectively, the effective permittivity is then

$$\varepsilon_p = \frac{1}{4}(\beta + \sqrt{\beta^2 + 8\varepsilon_d\varepsilon_w}), \tag{1}$$

with $\beta = (3\nu_d - 1)\varepsilon_d + (3\nu_w - 1)\varepsilon_w$. In general both ϵ_d and ϵ_w are complex and depend on frequency, although in practice we find that ϵ_d is real and independent of frequency over our measured bandwidth.

We obtain ε_d for specific paper types through a calibration procedure described below. For ε_w, we use a double Debye model [16–18],

$$\varepsilon_w(\omega) = \varepsilon_\infty + \frac{\varepsilon_s - \varepsilon_2}{1 - i\omega\tau_1} + \frac{\varepsilon_2 - \varepsilon_\infty}{1 - i\omega\tau_2}, \tag{2}$$

where ε_∞ is the limiting value of the high-frequency permittivity, ε_s is the static dielectric constant, ε_2 is the intermediate permittivity, and τ_1, and τ_2 are temperature-dependent time constants that are related to translational and rotational diffusion, hydrogen bond rearrangements, and structural rearrangement [18].

The transmission amplitude of the slab in air is then [19]

$$T(\omega;\boldsymbol{\theta}) \equiv \frac{E_t(\omega)}{E_i(\omega)} = \frac{t(\omega;\boldsymbol{\theta})t'(\omega;\boldsymbol{\theta})e^{i\beta(\omega;\boldsymbol{\theta})}}{1 + r(\omega;\boldsymbol{\theta})r'(\omega;\boldsymbol{\theta})e^{2i\beta(\omega;\boldsymbol{\theta})}}, \tag{3}$$

where $n = \sqrt{\epsilon_p(\nu_d)}$, $\beta = nh\omega/c$, $t = 2/(n+1)$, $t' = 2n/(n+1)$, $r = -r' = -(n-1)/(n+1)$, and the model parameters are written in vector notation $\boldsymbol{\theta} = [h, \nu_d]$. This model incorporates an infinite number of multiple reflections while our measurement time window is finite. In practice, however, with paper samples we expect an amplitude reduction of at least a factor of 25 for each successive reflection, causing the signal from multiple reflections to fall below the noise floor well before the end of the time trace.

We determine $\boldsymbol{\theta}$ from fits to terahertz time sequences taken with the sample, $\mathbf{y}^s = [y_1^s, y_2^s, ..., y_N^s]$, and without it, $\mathbf{y}^r = [y_1^r, y_2^r, ..., y_N^r]$. The fit procedure compares $\mathbf{y}^s$ to the model time trace $\mathbf{f}(\boldsymbol{\theta}; \mathbf{y}^r) = [f_1, f_2, ..., f_N]$ obtained by filtering the reference pulse $\mathbf{y}^r$ with the model transmission amplitude $T(\omega; \boldsymbol{\theta})$:

$$\mathbf{f}(\boldsymbol{\theta}; \mathbf{y}^r) = \mathcal{F}^{-1}\left(\{T(\omega_k; \boldsymbol{\theta}) \exp(-ih\omega_k/c)\mathcal{F}(\mathbf{y}^r)_k\}\right). \tag{4}$$

The factor $\exp(-ih\omega_k/c)$ compensates for the additional path length in air that the reference pulse must traverse relative to when the sample is present. The best fit parameters are then obtained by minimizing the cost function,

$$\mathrm{C}(\boldsymbol{\theta}; \mathbf{y}^{\mathrm{s}}, \mathbf{y}^{\mathrm{r}}) = \sum_k |y_k^s - f_k(\boldsymbol{\theta}; \mathbf{y}^r)|^2. \tag{5}$$

3. Measurements

All measurements are performed with a conventional THz time-domain spectrometer (EKSPLA). A fiber laser operating at 775 nm (TOPTICA) is used to trigger photoconducting GaAs antennae that yield a bandwidth of about 1.5 THz. The emitter is modulated with a 60 V, 70.0 KHz bias signal and the detector response is measured by a lock-in amplifier. We collect N = 2048 points separated by 0.02 ps intervals at a 4 Hz scan rate. The THz beam spot diameter at the sample is about 3 mm. A typical pair of reference and sample pulses is shown in Fig. 1. The residuals shown in the lower plot reveal that the measurements are described well by the model; however, the small correlated errors near the main pulse, at the level of 1% of the peak amplitude, suggest an avenue for future improvement.

We calibrate ε_d in two steps. First, the complex refractive index of an oven-dried sample is determined following the procedure described in [20]. Setting $\nu_d = 1$ and h to an independently measured value, a nonlinear least squares fit to Eq. 3 is performed to give the value of the complex index at each frequency. Following this procedure we have determined the complex refractive indices for two oven-dried samples: standard ‘photocopy’ paper, and ‘fine’ paper. We find that these refractive indices are real and constant over the bandwidth of our system: $n = 1.44 \pm 0.02$ and $n = 1.50 \pm 0.02$ for ‘photocopy’ and ‘fine’ paper, respectively. In principle these values can change slightly as the paper is moistened and the fiber morphology changes, so we perform a second calibration step on paper that has been moistened to the level expected for the sample of interest. With measurements on a sample of known thickness, we use Eq. 5 to determine h and vary the value of n until it agrees with its independently measured value. Based on our observations of oven-dried paper, we constrain n in this optimization to be real and independent of frequency. At equilibrium moisture level (under ambient conditions) near 5%, we obtained $n = 1.41 \pm 0.02$ and $n = 1.47 \pm 0.02$ for ‘photocopy’ and ‘fine’ paper, respectively. The small but significant reduction in index for both types of paper suggests that the paper fiber may change slightly with moisture. For closed-loop monitoring applications, however, the moisture variation is expected to be much smaller than 5%, and we estimate that the uncertainty resulting from moisture-dependent index changes will be smaller than the statistical uncertainty in h.

In the paper industry it is more common to control the moisture fraction M and the mass per unit area or basis weight B, rather than (h, ν_d). The moisture fraction is defined as $M \equiv \nu_w\rho_w/(\nu_w\rho_w + \nu_d\rho_d)$, where ρ_w and ρ_d are the densities of water and dry content, respectively . The basis weight is given by $B = (\nu_d\rho_d + \nu_w\rho_w)h$. Assuming $\nu_d + \nu_w = 1$, we can relate M to ν_d by the proportional relationship

$$\frac{1-\nu_d}{\nu_d} = \frac{\rho_d}{\rho_w}\frac{M}{1-M}. \tag{6}$$

To determine ρ_d/ρ_w we weigh a dry sample, moisturize it to $M = 60\%$, then periodically measure THz transmission traces and the overall weight as the paper dries to $M = 5\%$. We then determine ν_d from the THz transmission, and M from the weight measurements. Fig. 2 shows the results with a fit to Eq. 6. The scatter in the data is dominated by irreproducibility in positioning the sample for each measurement. The quality of the fit ($R^2 = 0.9983$) supports the assumption that ρ_d is constant over the entire range of moisture levels shown. A similar calibration for B would require samples that were not available for the present study, made from the same material but with different densities. Since our method is not restricted to paper we retain (h, ν_d) as our primary variables, using the calibration for M to relate our measurement uncertainty to industrial standards.

To characterize the measurement uncertainty, we obtained estimates of $[h, \nu_d]$ from repeated measurements on both samples, using the calibration parameters shown in Table 1. For each paper sample one reference pulse was paired with a hundred sample THz pulses acquired over 50 seconds.

Scatterplots of the parameter estimates, shown in Fig. 3, demonstrate a significant correlation between h and ν_d that results from the structure of our model. Eq. 3 depends exponentially on the product $hn(\nu_d)$, and a small overestimate of ν_d will result in an underestimate of $\Re\{n(\nu_d)\}$ that must be compensated by a corresponding overestimate of h. In principle, if $n(\nu_d)$ were real and frequency independent for all ν_d, then this correlation would make it impossible to estimate h and ν_d separately. In practice, however, the parameters are distinguishable because in our model both the frequency dependence and the imaginary part of n vary strongly with ν_d. The parameter uncertainties obtained from these measurements are summarized and compared to independent measurements in Table 2.

The precision in the parameters obtained using the terahertz sensor is comparable to existing on-line sensor technologies developed by Honeywell. For caliper measurements, the precision is required to be sub-micron, while the accuracy is considered relatively unimportant, so our precision of 0.5 μm and accuracy of 0.3 μm are satisfactory. In case of moisture sensors, both accuracy and precision are significant. For a typical Honeywell moisture sensor, the precision is about 0.1% while the accuracy is required to be 0.5% of absolute moisture. Our values of 0.35% precision and 1% accuracy are a bit larger than this, but as we will see below the fundamental limits on these uncertainties are an order of magnitude lower than in our measurements.

4. Monte Carlo simulations

Several types of noise are present in our system, and we have used Monte Carlo simulations to identify the current limits on the measurement uncertainty. We expect the basic contributions to our system noise to be additive noise from the electronics, multiplicative noise from laser power fluctuations, and time-base jitter from opto-mechanical vibrations. We expect all of these noise sources to exhibit a $1/f^\alpha$ noise spectrum at low frequencies, where f is the sampling frequency and $\alpha \sim 1$, and that at sufficiently high frequencies this will roll over to a white noise floor. We approximate this behavior with a step-like spectrum that drops from one constant value to a lower constant value as the frequency increases above the scan rate to get the following simplified model for adding noise to an ideal THz sequence $\{y_k\}$:

$$y_k \to [1 + a_1 X^{(1)} + a_2 X_k^{(2)}] y(t_k + a_3 X^{(3)} + a_4 X_k^{(4)}) + a_5 X_k^{(5)}. \tag{7}$$

Each X corresponds to a Gaussian random variable with zero mean and unit variance and each a is a coefficient that determines its contribution to the overall noise. On the right hand side of the expression, y is taken to be a continuous function of time so that the effect of jitter can be evaluated; in practice this is obtained from interpolation. The values of $X^{(1)}$ and $X^{(3)}$ are applied to all y_k in the sequence and correspond to low-frequency noise. The remaining terms correspond to high-frequency noise and have a white spectrum for each random sequence $\{X_k\}$. In this way the terms $a_1 X^{(1)}$ and $a_2 X^{(2)}$ correspond to low-frequency and high-frequency multiplicative noise, respectively; $a_3 X^{(3)}$ and $a_4 X^{(4)}$ correspond to low-frequency and high-frequency jitter; and $a_5 X^{(5)}$ corresponds to high-frequency additive noise. We omit low-frequency additive noise because this would simply shift each sequence up or down by a constant and not lead to variation in the fit parameters.

To characterize the system noise quantitatively, we collect one hundred sample pulses $\{\mathbf{y}^{(1)}, \mathbf{y}^{(2)}, \ldots, \mathbf{y}^{(100)}\}$ and calculate the standard deviation of the data set at each time value, $s_k = \mathrm{stdev}(\{y_k^{(1)}, y_k^{(2)}, \ldots, y_k^{(100)}\})$. We expect the resulting time sequence $\mathbf{s}$ to be proportional to the magnitude of the pulse slope for temporal jitter, proportional to pulse magnitude for multiplicative noise, and independent of time for additive noise. The results are shown in

Fig. 4 and reveal two peaks where the pulse is steepest, indicative of temporal jitter. Some multiplicative noise must also be present because the standard deviation near the peak of the THz pulse is slightly higher than the baseline, even though the slope of $\mathbf{y}$ is zero there. To determine the coefficients a_j we simulate one hundred noisy pulses using Eq. 7, calculate their time-dependent standard deviation in the same way as the experimental traces, and adjust the a_j to obtain the best least-squares fit between the experimental noise trace and the simulated one. We find that out of the five parameters, only three contribute significantly: low frequency multiplicative noise ($a_1 = 0.00236$), low-frequency jitter ($a_3 = 1.94$ fs), and high-frequency additive noise ($a_5 = 2.027$ mV).

Further simulations allow us to estimate the influence of each of these noise terms on the parameter estimates. Fig. 5 shows a schematic of the procedure. Using Eqs. 3 and 7, a noisy transmitted pulse with ideal parameters $\boldsymbol{\theta}_{id}$ is simulated in the lower part of the schematic, and a model pulse with fit parameters $\tilde{\boldsymbol{\theta}}$ is simulated in the upper part of the schematic. A least-squares fit procedure is then used to optimize $\tilde{\boldsymbol{\theta}}$. The results for the noise model obtained from Fig. 5 are shown in Fig. 6(a), and matches closely the experimentally observed behavior for the photocopy paper sample. The contributions of different noise terms to the parameter uncertainties are outlined in Table 3, and show that the most significant source of uncertainty in our system is due to low frequency jitter.

It is now possible to characterize the fundamental limitations on the measurement uncertainties by considering only the additive noise with $SNR = 1000$, a typical value. The contours in Fig. 6(b) correspond to 99, 95, 90, and 68% confidence intervals calculated using the covariance matrix [21] and show that we can hope to decrease the uncertainties further by an order of magnitude by improving the multiplicative and jitter noise.

The uncertainties in thickness and volume fraction for various samples along with their corresponding correlation coefficients are calculated and presented in Table 4.

5. Conclusions

We have developed a procedure to measure the thickness and composition of paper simultaneously using a conventional time-domain THz spectrometer. Previous work has focused on measuring these parameters independently. However, simultaneous measurements that yield equal-time correlations between the parameters are of much greater value for practical control applications. Our model uses a Bruggeman effective medium theory to model the mixture of dry contents and water in paper. Work is under way to investigate other effective medium theories for modeling the terahertz response of paper.

As a proof of principle, we applied our methodology to two different paper samples. In case of caliper, our precision and accuracy surpasses that of conventional sensors by a factor of two, while for moisture, the terahertz sensor performance is equivalent to that of conventional sensors. We have developed a noise model and used it to characterize our measurement precision through Monte Carlo simulations. We discovered that the dominant noise in our system is low-frequency jitter, and that by minimizing it we could increase the precision by an order of magnitude. Work is in progress to measure reference and sample pulses simultaneously to reduce this jitter.

For industrial paper processing applications, simultaneous measurement of the three fundamental paper parameters—caliper, moisture, and basis weight—is of great interest. In this work we focused on measurements of caliper and dry content volume fraction because the method is not restricted to paper and these are the quantities most directly accessible in our measurement. To obtain moisture and basis weight, further calibration steps are required to make an empirical link between the dry refractive index and density. We have shown that this provides good results for moisture measurements. To perform the required calibration for basis weight measurements, samples made from the same material but with different densities are required. Future work on suitable samples will address this.

6. Acknowledgement

This work is funded in part by NSERC (Natural Sciences and Engineering Research Council of Canada), and by CIFAR (Canadian Institute for Advanced Research). PM acknowledges support from an NSERC Industrial Postgraduate Scholarship.

References

[1] D. Mittleman, ed., *Sensing with Terahertz Radiation* (Springer, 2004).

[2] G. Grüner, ed., *Millimeter and Submillimeter Wave Spectroscopy of Solids* (Springer, 1998).

[3] R. E. Miles, X. C. Zhang, H. Eisele, A. Krotkus, eds., *Proceedings of the NATO Advanced Research Workshop on Terahertz Frequency Detection and Identification of Materials and Objects* (Springer, 2007).

[4] A. G. Markelz, A. Roitberg, and E. J. Heilweil, "Pulsed terahertz spectroscopy of DNA, bovine serum albumin and collagen between 0.1 and 2.0 THz," Chem. Phys. Lett. **320**, 42–8 (2000).

[5] M. Walther, B. Fischer, M. Schall, H. Helm, and P. Uhd Jepsen, "Far-infrared vibrational spectra of all-*trans*, 9-*cis*, and 13-*cis* retinal measured by THz time-domain spectroscopy," Chem. Phys. Lett. **332**, 389–95 (2000).

[6] K. Lien Nguyen, T. Friščić, G. M. Day, L. F. Gladden, and W. Jones, "Terahertz time-domain spectroscopy and the quantitative monitoring of mechanochemical cocrystal formation," Nat. Mater. **6**, 206–9 (2007).

[7] K. Kogermann, J. A. Zeitler, J. Rantanen, T. Rades, P. F. Taday, M. Pepper, J. Heinämäki, and C. J. Strachan, "Investigating Dehydration from Compacts Using Terahertz Pulsed, Raman,and Near-Infrared Spectroscopy," Appl. Spectrosc. **61**, 1265–74 (2007).

[8] M. Yamaguchi, F. Miyamaru, K. Yamamoto, M. Tani, and M. Hangyo, "Terahertz absorption spectra of L-, D-, and DL-alanine and their application to determination of enantiometric composition," Appl. Phys. Lett. **86**, 053903 (2005).

[9] C. J. Strachan, P. F. Taday, D. A. Newnham, K. C. Gordon, J. A. Zeitler, M. Pepper, and T. Rades, “Using terahertz pulsed spectroscopy to quantify pharmaceutical polymorphism and crystallinity,” J. Pharm. Sci. **94**, 837–46 (2005).

[10] M. Naftaly, A. P. Foulds, R. E. Miles, and A. G. Davies, “Terahertz transmission spectroscopy of nonpolar materials and relationship with composition and properties,” Int. J. Infrared Millimeter Waves **26**, 55–64 (2005).

[11] K. Cutshall, “Cross-directional control,” in *Paper Machine Operations. (Pulp and Paper Manufacture Series, 3rd ed., Vol. 7)*, B. A. Thorp and M. J. Kocurek, ed., (Atlanta and Montreal, 1991), pp. 472–506.

[12] D. Banerjee, W. von Spiegel, M. D. Thomson, S. Schabel, and H. G. Roskos, “Diagnosing water content in paper by terahertz radiation,” Opt. Express **16**, 9060–9066 (2008).

[13] F. Huang, J. F. Federici, and D. Gary, “Determining thickness independently from optical constants by use of ultrafast light,” Opt. Lett. **29**, 2435–2437 (2004).

[14] T. D. Dorney, R. G. Baraniuk, and D. M. Mittleman, “Material parameter estimation with terahertz time-domain spectroscopy,” J. Opt. Soc. Am. A **18**, 1562–1571 (2001).

[15] T. C. Choy, *Effective Medium Theory: Principles and Applications (International Series of Monographs on Physics)* (Oxford, 1999).

[16] J. K. Vij, D. R. J. Simpson, and O. E. Panarina, “Far infrared spectroscopy of water at different temperatures: GHz to THz dielectric spectroscopy of water,” J. Mol. Liq. **112**, 125–135 (2004).

[17] C. N. Thrane, P. O. Astrand, A. Wallqvist, K. V. Mikkelsen, and S. R. Keiding, “Investigation of the temperature dependence of dielectric relaxation in liquid water by THz reflection spectroscopy and molecular dynamics simulation,” J. Chem. Phys. **107**, 5319–5331 (1997).

[18] E. Pickwell, B. E. Cole, A. J. Fitzgerald, V. P. Wallace, and M. Pepper, “Simulation of terahertz pulse propagation in biological systems,” Appl. Phys. Lett. **84**, 2190–2192 (2004).

[19] M. Born, and E. Wolf, *Principles of Optics* (Pergamon, 1964), 2nd Ed., 51–63.

[20] L. Duvillaret, F. Garet, and J. L. Coutaz, “A Reliable Method for Extraction of Material Parameters in Terahertz Time-Domain Spectroscopy,” IEEE J. Sel. Top. Quant. Electron. **2**, 739–745 (1996).

[21] P. C. Gregory, *Bayesian Logical Data Analysis for the Physical Sciences* (Cambridge, 2005).

List of Figure Captions

Fig. 1. A typical set of reference (dashed line) and sample (solid line) pulses and their corresponding spectra. The residual of a typical fit is shown in the bottom figure.

Fig. 2. Calibration of ρ_d/ρ_w. Measurements of moisture fraction M determined by weight are plotted against $\nu_d/(1-\nu_d)$ determined from THz measurements (●), together with the fit to Eq.6 with $\rho_d/\rho_w = 0.87$ (dashed line).

Fig. 3. (Color online) Experimental scatter plots or ν_d and h resulting from repeated THz measurements on the same spot on a sample for (a) photocopy paper and (b) fine paper.

Fig. 4. Measured and simulated noise in the time domain. Solid lines show the standard deviations of a set of hundred pulses generated by Monte Carlo simulation (top) and by the experimental apparatus (bottom). For clarity the simulation noise curve offset upward from the experimental curve. For comparison the dotted line shows a typical signal curve, scaled down by a factor of 60.

Fig. 5. Monte Carlo simulation of the parameter estimates. An ideal input signal pulse $\mathbf{y_i}$, shown at the left, is used to generate two simulated transmitted pulses, $\mathbf{y}$ and $\tilde{\mathbf{y}}$. The pulse $\tilde{\mathbf{y}}$ is the convolution of $\mathbf{y_i}$ with the transmittance function with estimated parameters $\tilde{\boldsymbol{\theta}}$ and no noise added, and $\mathbf{y}$ is the convolution of $\mathbf{y_i}$ with the transmittance function using ideal parameters $\boldsymbol{\theta}_{id}$, with noise added with the function $\boldsymbol{\eta}$ according to Eq. 7. The best fit parameters are estimated by minimizing the norm squared difference between two transmitted pulses, as shown on the right.

Fig. 6. (Color Online) Monte Carlo simulation of h and ν_d estimates for fine paper, with (a) $a_1 = 0.0024$, $a_5 = 2.027$ mV, $a_3 = 1.95$ fs, and $a_2 = a_4 = 0$, and with (b) $a_5 = 1.5$ mV and $a_1 = a_2 = a_3 = a_4 = 0$. In (b), the true value of the parameters is shown at the center in red

(♦), and the elliptical contours represent 99, 95, 90, and 68% confidence regions. Note the scale difference between (a) and (b).

7. Figures

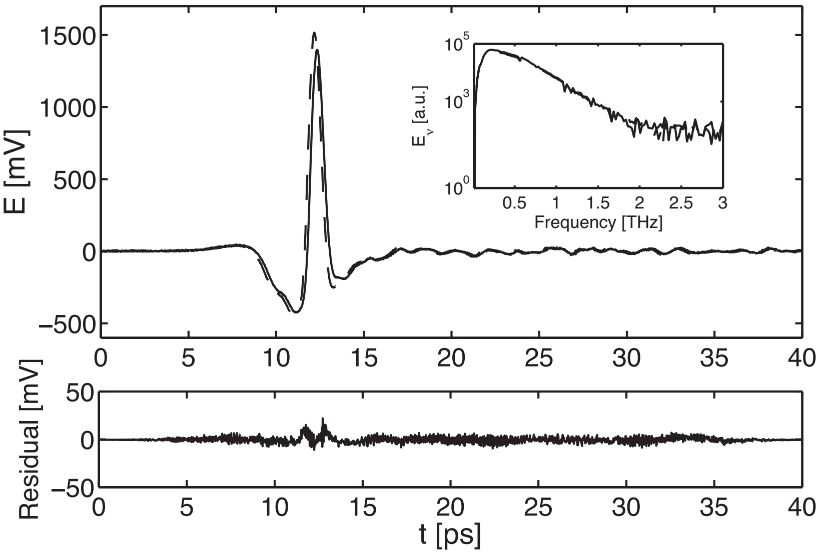

Fig. 1.

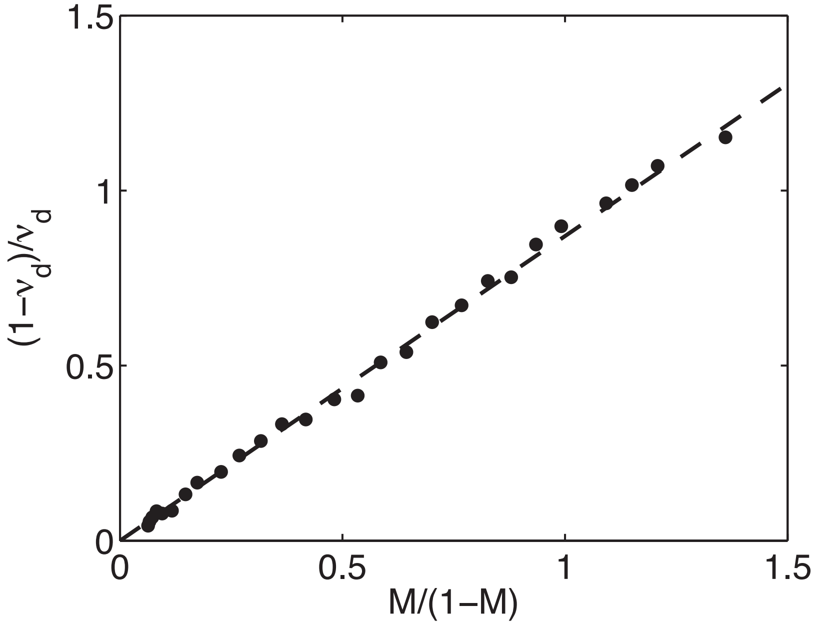

Fig. 2.

8. Tables

Table 1. Calibration parameters used for photocopy and fine paper samples.

	n_r	ρ_d/ρ_w
Photocopy	1.41	0.87
Fine	1.47	1.0

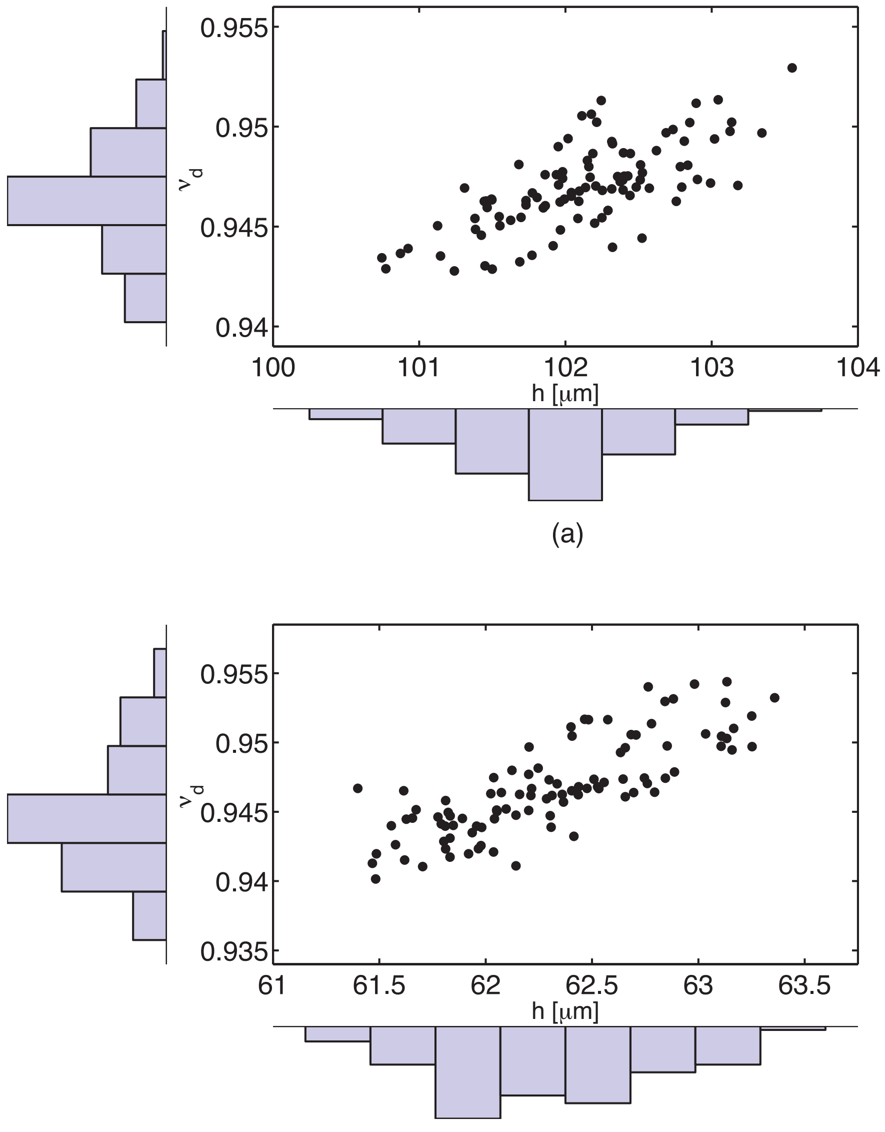
0.955
0.95
0.945
0.94
ν_d
100
101
102
103
104
h [μm]
0.955
0.95
0.945
0.94
0.935
ν_d
61
61.5
62
62.5
63
63.5
h [μm]

(a)

(b)

Fig. 3.

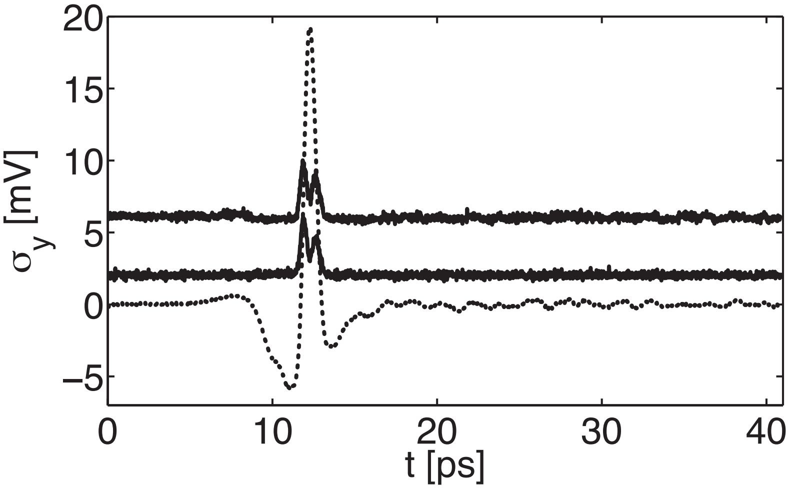
20
15
10
5
0
−5
σ_y [mV]
0
10
20
30
40
t [ps]

Fig. 4.

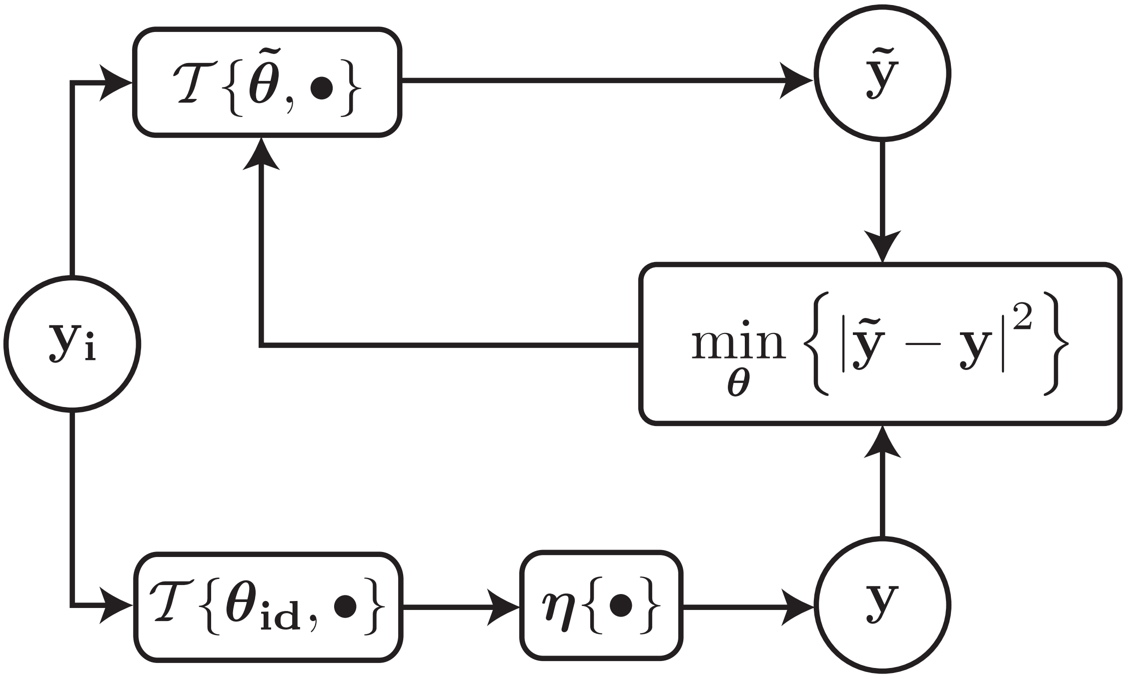
$\mathcal{T}\{\tilde{\boldsymbol{\theta}}, \bullet\}$
$\tilde{\mathbf{y}}$
$\mathbf{y_i}$
$\min_{\boldsymbol{\theta}} \left\{ |\tilde{\mathbf{y}} - \mathbf{y}|^2 \right\}$
$\mathcal{T}\{\boldsymbol{\theta}_{\mathbf{id}}, \bullet\}$
$\boldsymbol{\eta}\{\bullet\}$
$\mathbf{y}$

Fig. 5.

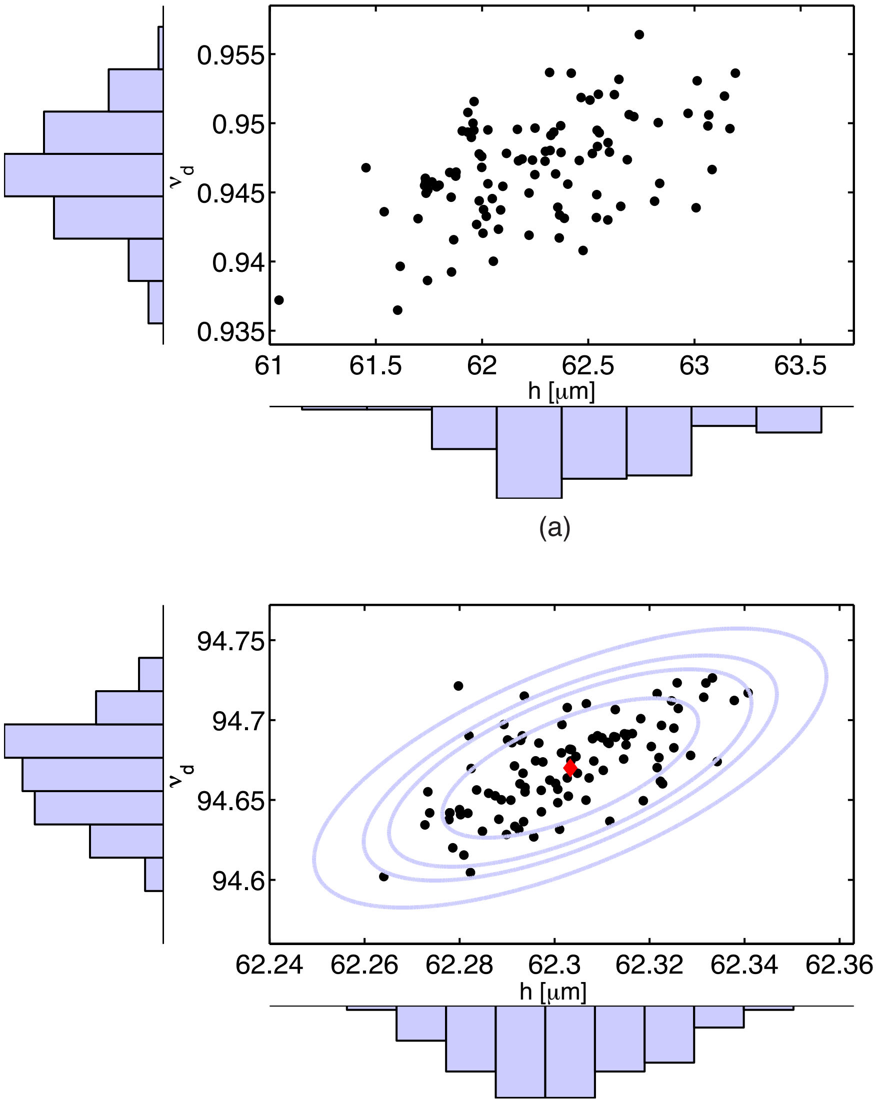
0.955
0.95
0.945
0.94
0.935
ν_d
61
61.5
62
62.5
63
63.5
h [μm]
94.75
94.7
94.65
94.6
ν_d
62.24
62.26
62.28
62.3
62.32
62.34
62.36
h [μm]

(a)

(b)

Fig. 6.

Table 2. Paper parameters measured using THz and by independent methods. For the independent measurements, the thickness is measured using a standard bench-top TAPPI caliper gauge while a scale is used to measure both the percent moisture and the basis weight. The uncertainties correspond to 68% confidence levels.

	THz		Independent	
	$h(\mu\text{m})$	$M(\%)$	$h(\mu\text{m})$	$M(\%)$
Photocopy	102.12 ± 0.58	6.04 ± 0.25	102.0	5.91
Fine	62.30 ± 0.49	5.47 ± 0.35	62.6	6.44

Table 3. Noise simulation and uncertainties – J: jitter noise, M: multiplicative noise, W: white noise.

	Simulation							Experiment
	MJW	MW	JW	JM	J	M	W	
$\sigma_h(\mu\text{m})$	0.43	0.15	0.41	0.43	0.41	0.15	0.036	0.49
$\sigma_\nu(\times 10^{-3})$	3.8	3.8	0.93	3.8	0.75	3.8	0.56	0.97

Table 4. Simulated uncertainties and correlation coefficients assuming only white Gaussian noise.

	$\sigma_h(\times 10^{-2}\mu m)$			$\sigma_{\nu_d}(\times 10^{-2}\%)$			corr(h, ν_d)		
	ν_d								
	0.3	0.6	0.9	0.3	0.6	0.9	0.3	0.6	0.9
h (μm)									
70	2.2	1.9	1.8	3.9	2.9	2.6	0.57	0.51	0.61
100	2.4	2.0	1.8	3.6	2.6	2.1	0.63	0.52	0.58
200	4.3	2.6	2.0	3.3	1.9	1.4	0.77	0.70	0.73